Stable Parking Control of a Robot Astronaut in a Space Station Based on Human Dynamics

Zhihong Jiang, Jiafeng Xu, Hui Li* and Qiang Huang, *Fellow*, *IEEE*

***Abstract*—Controlling a robot astronaut to move in the same way as a human astronaut to realize a wide range of motion in a space station is an important requirement for the robot astronauts that are meant to assist or replace human astronauts. However, a robot astronaut is a nonlinear and strongly coupled multibody dynamics system with multiple degrees of freedom, whose dynamic characteristics are complex. Therefore, implementing a robot astronaut with wide-ranging motion control in a space station is a tremendous challenge for robotic technology. This paper presents a wide-ranging stable motion control method for robot astronauts in space stations based on human dynamics. Focusing on the astronauts' parking motion in a space station, a viscoelastic dynamic humanoid model of parking under microgravity environment was established using a mass-spring-damper system. The model was used as the expected model for stable parking control of a robot astronaut, and the complex dynamic characteristics were mapped into the robot astronaut system to control the stable parking of the robot astronaut in a manner similar to a human astronaut. This provides a critical basis for implementing robots that are capable of steady wide-ranging motion in space stations. The method was verified on a dynamic system of a robot astronaut that was constructed for this research. The experimental results showed that the method is feasible and effective and that it is a highly competitive solution for robot astronauts with human-like moving capabilities in space stations.**

***Index Terms*—Robot astronaut, Motion control, Spring-damper system, Model mapping and controlling**

I. Introduction

BECAUSE space robots are not restricted by the human physiological conditions [1] that make the space environment harsh on humans, their use to assist or replace astronauts in space exploration is the probable choice for space station development [2], [3]. Because robot astronauts have the appearance of astronauts, there is no need to change the structural environment of the space station. Controlling robots to move like human astronauts in the space station environment with a wide range of motion is an effective approach for assisting or replacing astronauts [4].

"Wide-ranging motion" means that the robot moves freely in the space station that is similar to that of an astronaut, and is used to distinguish the robot movement through a given orbit or through the use of a climbing handrail [5], [6], [7]. However, the issue of stable wide-ranging motion of space robots in space stations has not been effectively solved. Currently, the main robots used at the International Space Station are the Robonaut series from the US [8], [9], Canadarm 2 from Canada [10], [11], and Eurobot from the European Space Agency (ESA) [12]. Robonaut has a similar appearance to humans and thus can carry out a specific range of motion in the space station by crawling along special handrails. Canadarm 2 performs a wide range of motions through the use of specific rails and fixed electromechanical interfaces. Eurobot moves outside the space station by firmly gripping onto the rails of the station and alternating the motion of its arms. The Beijing Astronaut Robot [13], which was developed autonomously by the Beijing Institute of Technology, performs wide-ranging motion in the space station by gripping onto handrails with three coordinated arms and specific guiding rails. All of these space robots have increased the requirements for the structure of the space station, which has increased the system complexity of the space station. In addition, the motion efficiency of the current space robots is low, and their ranges of motion are limited. Currently, the primary mechanism of motion for robot astronauts is gripping onto the handrails of the space station [14], [15]. To facilitate the motion and operation of astronauts in the space station cabin, the rigid handrails used by robots for climbing are sparse, which results in difficulty for robot astronauts to have a wide range of motion for handrail climbing; therefore, the ability of the robot to assist in the astronauts' operations is extremely limited. This has also limited the ability of the robots to replace astronauts in carrying out space station duties.

Astronauts can move their bodies back and forth, turn and park by pushing on the handrails and bulkheads, so the motion of astronauts in the space station is free, rapid, stable and wide-ranging. Therefore, a new wide-ranging motion mechanism is proposed. Assuming that the basic structure of the space station does not change, wide-ranging motion of robot astronauts in the space station can be realized by controlling the robot astronaut to have the dynamic characteristics of a human astronaut in the space station. The modes of motion of astronauts in the space

This work were supported by the National Key Research and Development Program of China (2018YFB1305300) and the National Natural Science Foundation of China (61733001, 61573063, 61873039, U1713215). (Corresponding author: Hui Li, lihui2011@bit.edu.cn).

The authors are with the School of Mechatronic Engineering, Advanced Innovation Center for Intelligent Robots and Systems, Key Laboratory of Biomimetic Robots and Systems of Chinese Ministry of Education, Beijing Institute of Technology, Beijing 100081, China (e-mail: jiangzhihong@bit.edu.cn; 2235797879@qq.com; lihui2011@bit.edu.cn; qhuang@bit.edu.cn).

station mainly include starting, flying, and parking. Parking is defined as the contact between the arm of the astronaut and the space station at a certain velocity to implement stable body docking for operations or to change the motion mode. It is an important motion mode for astronauts in space. Parking involves the contact dynamics between the arm and the space station, which are more complicated than the dynamics of starting and flying. Therefore, this paper focuses on humanoid robot parking.

The state of the robot's motion is sensitive to internal structural forces, joint friction, environmental contact forces and external disturbances under microgravity. Its dynamic characteristics are complicated, which makes it difficult to control robot astronauts to perform parking that resembles that of an astronaut under microgravity. The existing control theories of humanoid robots mainly focus on the modeling of robotic legs, which resolves the motion control issues of robotic feet on the ground. Shahbazi, Babuška and Lopes [16] developed a bipedal spring-loaded inverted pendulum (SLIP) model for humanoid robots, which performed a robotic transformation between three motion modes (i.e., active running, walking and walk-run). Motoi et al. [17] proposed a bipedal model method based on a virtual linear inverted pendulum (VLIP) to obtain the expected center of gravity (COG) position of the robot and the foot placement. Hwang and Inohira [18] made use of virtual spring-damping in bipedal modeling of humanoid robotic legs, which was successful in providing stable control of a robot climbing stairs. In the microgravity environment, the parking of an astronaut is a process that involves gaining stability through contact [19] between the arms and a handrail. The dynamic modeling theory of an on-ground humanoid robot cannot reflect the dynamic characteristics of arms in the case of astronaut parking, so it is difficult to control the parking of a humanoid robot astronaut. This paper presents a stable parking control method for robot astronauts based on human-body parking dynamics. The method models the dynamic characteristics of human arms under microgravity. By setting up an actual physical model, the model parameters are actively adjusted to fit the dynamic characteristics of the human arm during parking to obtain a dynamic model with a similar dynamic response to that of the human arm. The human-arm dynamic model is then applied to the parking control of a robot astronaut to achieve high-level stable parking by the humanoid robot astronaut.

The main idea of this paper is to propose the dynamic model of human under microgravity as the expected control model of the robot to realize the free movement of the robot astronaut in the space station. The parking motion control is selected to verify the validity and achievability of the proposed method. The technical approach is to give a robot astronaut the same dynamic characteristics as a human astronaut by means of humanoid control so the rigid robotic arm can exhibit the same flexibility as that of a human arm and perform stable and safe parking similar to that of a human astronaut in a space station. Specifically, a dynamic data acquisition system is established based on the interactions between a human and the environment when the astronaut makes wide-ranging motion under microgravity. The dynamic data from the interactions between the handrail and the astronaut during parking are then obtained. By analyzing the dynamic characteristics of the astronaut parking process, a physical model based on a spring-damper system [20], [21] was selected to model the dynamics of the arms [22] during parking and develop an expected model of parking control for a robot astronaut. The complete dynamic mapping from the expected model to the robot astronaut was realized by normal contact force mapping and tangential parking control and velocity mapping based on PD feedback control. According to the equivalence law of dynamic responses, a robot astronaut can behave like an astronaut after complete mapping of the dynamic characteristics of the interactions between the human arm and a handrail during parking, which thus achieves the control of stable parking of a humanoid robot astronaut. The core idea of the control system is shown in Fig. 1.

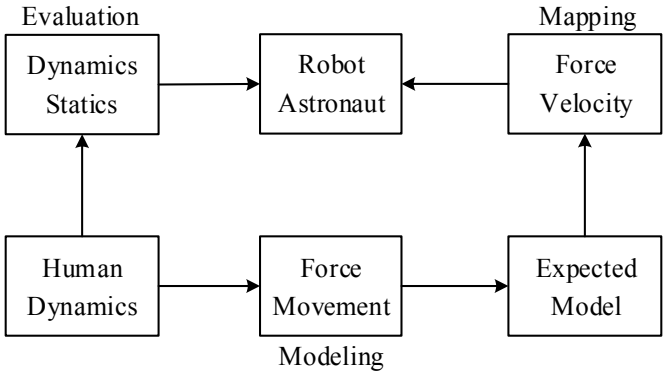

Fig. 1. Humanoid parking control process of a robot astronaut.

The structure of the remainder of this paper is as follows. In Section II, we collect the dynamic characteristics data of astronaut parking under microgravity and model the dynamics of human arms to obtain the expected parking control model. In Section III introduces the mathematical mapping from the expected model to the robot astronaut control model, which mainly includes normal contact force mapping, tangential parking control and real-time velocity mapping. Section IV provides a method for evaluating the results of robot astronaut parking using the dynamic characteristics of astronaut parking as the standard. In Section V, the robotic astronaut's humanoid parking, the control system robustness and the adaptivity of the control system with XY initial velocities are verified experimentally. Finally, a summary of the research and the conclusions of the paper are given in Section VI.

II. Dynamic Modeling Of Human Body Parking

The experiments of human parking under microgravity were designed based on an experimental platform of a simulated microgravity environment. Dynamic characteristics data were also collected in the experiment. Through human-body data analysis, the human arms were abstracted as a mass-spring-damper system based on the equivalence law of dynamic responses to develop a dynamic model of human arms.

A. Dynamic Characteristics of Human Parking under Microgravity

One distinctive characteristic of the conditions in space is microgravity; therefore, the human parking dynamics data must also be obtained under microgravity, which is difficult for general experimental acquisition systems on the ground. The parking of the humanoid robot in this study involves many dynamic parameters, such as the contact force, motion velocity, joint velocity and body position, which increase the complexity of the data acquisition system. We constructed an astronaut parking dynamics data acquisition system that consists of a two-dimensional air floating platform, a motion capture system and a mechanical detection system, as shown in Fig. 2.

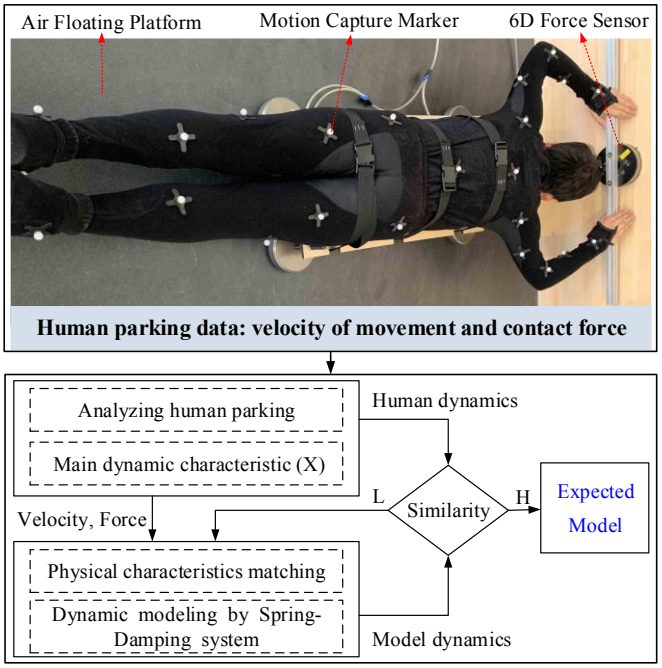

Fig. 2. Framework of human parking dynamics modeling and human parking data acquisition experiment. H indicates high similarity and L indicates low similarity. See the equation 28 for the calculation method. High similarity means that the absolute error of the two models is less than 10%.

The human parking experiment simulates the spatial microgravity environment through a two-dimensional air floating platform. The experimenter is fixed on a horizontally placed flat plate supported by four air floating discs. The total mass of the human and the air flotation device is 80.0 kg, where the human mass is 71.8 kg, and the flotation device mass is 8.2 kg. The human parking experiment mainly collected velocity and contact force data. The contact force data between the human hand and the handrail was collected by ATI's Omega 160 six-dimensional force sensor. The displacement of the human torso was collected by the Motion Analysis's Hawk-24 digital motion capture system. The torso velocity can be obtained from the torso displacement, and the length of the arms can be used to calculate the angle of each joint in the parking.

By analyzing the human parking movement, it is found that human's main velocity is perpendicular to the contact surface during parking movement, and the velocity in other directions is very small. The dynamic characteristics, such as contact force and velocity, are mainly reflected in this direction (Defined as the X direction). Therefore, mainly analyzed the human parking data perpendicular to the contact surface. At the same time, due to the completely symmetric distribution of the arms of the experimenter, the dynamic characteristics in this chapter are given by the left arm. The results of several contact force measurements at different parking velocities are shown in Fig. 3.

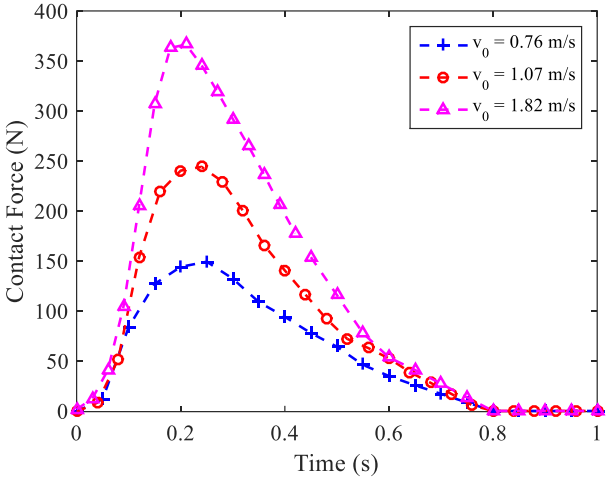

Fig. 3. Variations in the contact force at the end of the arm during parking experiments at different velocities.

The body positions during the parking experiments are shown in Fig. 4.

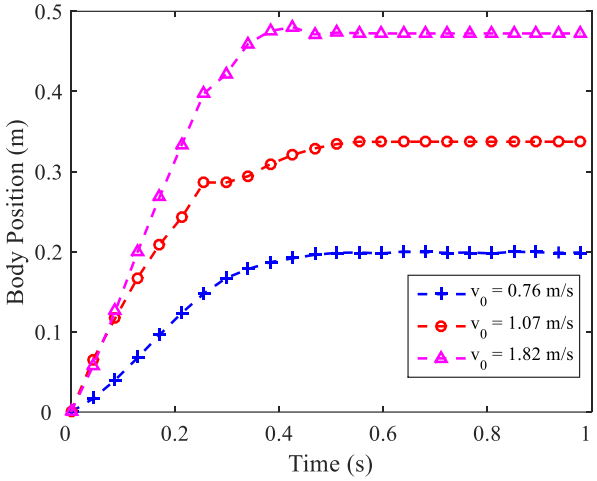

Fig. 4. Variations of the body position during parking experiments at different velocities. When the human body was in contact with the platform, we set the torso position to be the system origin, so the curve starts from zero.

B. Dynamic Model of the Human Body in the Parking Experiment

The collected dynamics data of the human body during parking were mathematically analyzed. Fig. 3 and Fig. 4 show that the contact force and the body position both increase at nearly the same rate within 0.2 seconds prior to parking. The contact force and body position data from 0 to 0.2 s are shown in Fig. 5.

At the same order of magnitude, the body position and contact force of the human body increase nearly the same from 0 to 0.2 s, which satisfied Hooke's law, that is:

$$f_{contact} = kx \tag{1}$$

where k is the equivalent stiffness of the arm, x is the displacement of the torso. An analysis of the dynamic characteristics shows that the human arm is equivalent to a spring in this stage; the spring is compressed as the body moves forward, and the kinetic energy of the human torso is transformed into the elastic potential energy of the spring.

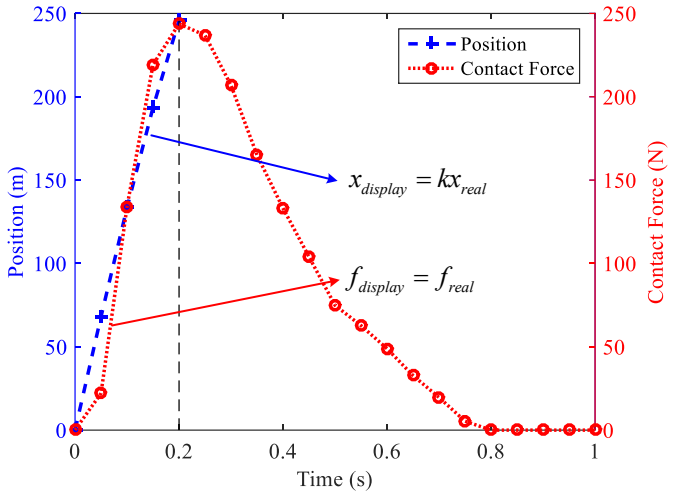

Fig. 5. Position and contact force of the human body during parking. To intuitively observe the relationship between the contact force and the body position, the characteristics of the body position are scaled up by 1000 times in the figure.

Fig. 3 and Fig. 4 indicate that the body velocity (Obtained by displacement data) decreases to 0 from 0.2 to 0.8 s, and the contact force decreases constantly during this stage. The contact force and body velocity data are shown in Fig. 6.

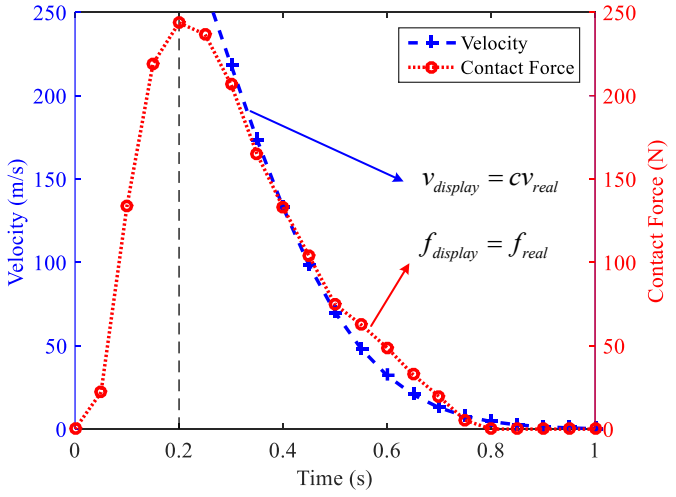

Fig. 6. Velocity and contact force of the human body during parking. To intuitively observe the characteristics of the contact force and velocity, the velocity data are scaled up by 100 times in the figure.

From 0.2 to 1.0 s, the velocity and contact force of the human body had similar variation patterns. Numerically, both values satisfied the following equation:

$$f_{contact} = cv \tag{2}$$

where c is the equivalent damping of the arm and v is the velocity of the torso. An analysis of the dynamic characteristics from 0.2 to 1.0 s shows that the human arm behaves as a viscous damper with a damping coefficient c. The elastic potential energy of the spring and the kinetic energy of the body are transformed into the internal energy through the viscous effect [23] of damping until the body velocity becomes zero and thus reaches a steady state.

During the parking process, the human arms exhibit some elasticity as well as damping characteristics due to the contact force. The astronaut parking process can be interpreted as a dynamic coupling between a spring, damper, mass and external force [24], [25]. The spring is responsible for buffering the collision impact force. The damper is used to prolong the collision time, which quickly consumes the kinetic energy of the mass prior to the collision. The mass-spring-damper system (Fig. 7) is applied to model the dynamics of the human body parking process.

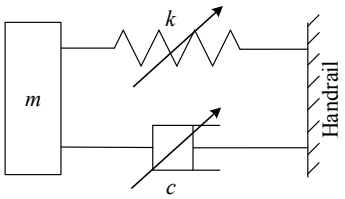

Fig. 7. Diagram of the mass-spring-damper system. The parameter m is equivalent to the total mass of the human body and the air floating device, k is the spring stiffness coefficient, and c is the damping coefficient.

The dynamic equation of the system [26] is as follows:

$$m\ddot{x} + c\dot{x} + kx = f_{contact} \tag{3}$$

where $f_{contact}$ is the reaction force exerted on the mass by the handrail.

Assume that the spring-damper system has an initial state $x_{t=0} = 0,\ \dot{x}_{t=0} \neq 0,\ \ddot{x}_{t=0} = 0$. At this point, the momentum of the entire system is $m\dot{x} \neq 0$. When the system is in contact with the handrail, according to the momentum theorem, we have the following:

$$f_{contact}\Delta t = \sum (m_i v_i^{t+\Delta t} - m_i v_i^t) \tag{4}$$

where Δt is the sampling interval.

The impulse of the reaction force from the handrail eventually attenuates the momentum of the system to zero, and $\ddot{x} = 0$; at this moment, the system has reached a steady state, as follows:

$kx_{t=t_d} = f_{external} = 0$ is true when $x_{t=0} = 0,\ \dot{x}_{t=0} \neq 0,\ \ddot{x}_{t=0} = 0$, where t_d is the system stabilization time during the parking, therefore, we have the following:

$$k_{t=0} \neq 0, k_{t=t_d} = 0. \tag{5}$$

When $t = 0, f_{contact} = 0$, according to the initial conditions, this gives the following:

$$c\dot{x} = 0 \tag{6}$$

where $\dot{x} \neq 0$, so $c_{t=0} = 0$

According to the theorem of the conservation of energy, the spring-damper system and the human body have the same initial and final kinetic energies, thus,

$$\frac{1}{2}m\dot{x}_0^2 - \frac{1}{2}k\Delta x^2 = \int_{t=0}^{t_d} c\dot{x} \tag{7}$$

where $\Delta x = x_{t=t_d} - x_{t=0}$, this formula is satisfied at any stage of the parking process, so we have the following:

$$c_{t=0} = 0,\ c_{t=t_d} \neq 0. \tag{8}$$

In summary, based on the variations in the stiffness and damping coefficient of the spring-damper system, human body parking can be divided into two stages and simulated separately by spring-damper systems with different characteristics. The first stage is the elastic stage with a duration of $t = 0 \sim t_s$, in which the arm mainly exhibits spring elasticity. Shown in Fig. 5, the contact force rises almost in a straight line until it reaches a maximum, according to the following equation:

$$k_{t=0\sim t_s} = \frac{f_{\max}}{x_h} \tag{9}$$

where x_h is the measured torso displacement when the contact force reaches the maximum. The system does not exhibit damping characteristics at this stage, so $c_{t=0\sim t_s} = 0$. From this, the first stage values of k, c in (3) can be obtained.

The dynamical properties of the system at t_s are transformed from elastic to damping properties, and $t_s = 0.75t_h$, where t_h is the moment when the contact force is at the maximum, according to the continuity of the contact force, the damping at time t_s is calculated as the following equation:

$$c_{t_s} = \frac{kx_{t_s}}{v_{t_s}} \tag{10}$$

where x_{t_s} is the displacement of the human at time t_s, and v_{t_s} is the velocity of the human at time t_s.

The second stage is the damping stage with a duration of $t = t_s \sim t_d$, in which the arm's elasticity is completely lost, mainly characterized by the damping characteristics of linear growth. The damping growth slope s_c can be calculated by the law of conservation of momentum:

$$s_c = \frac{mv_{t_s} - \int_{t_s}^{t_d} c_{t_s} v dt}{\int_{t_s}^{t_d} tvdt} \tag{11}$$

where v is the velocity of the torso during human parking. The stiffness of the system at this stage is zero, so $k_{t=t_s\sim t_d} = 0$.

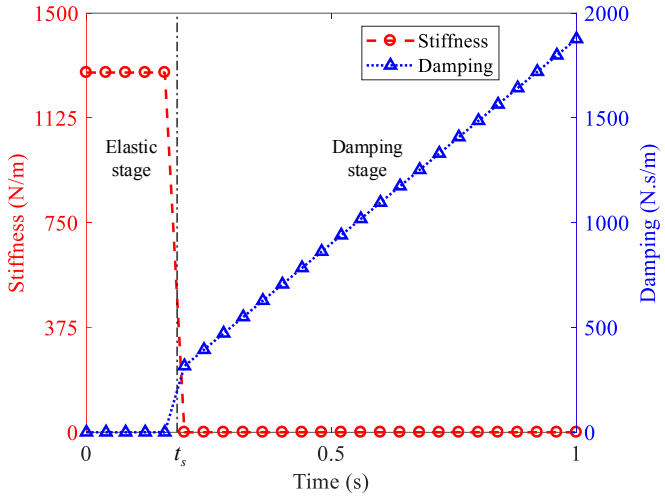

Fig. 8. Variations of the stiffness and damping coefficient in the spring-damper system during humanoid dynamics modeling.

The values of *m, c, k* determined according to the above method can give good modeling results. In the humanoid model, the variations of the stiffness and damping in the spring-damper system are shown in Fig. 8.

At this point, the characteristics of the dynamic model that was developed from the spring-damper system are similar to those of the human body during parking, as shown in Fig. 9 and Fig. 10.

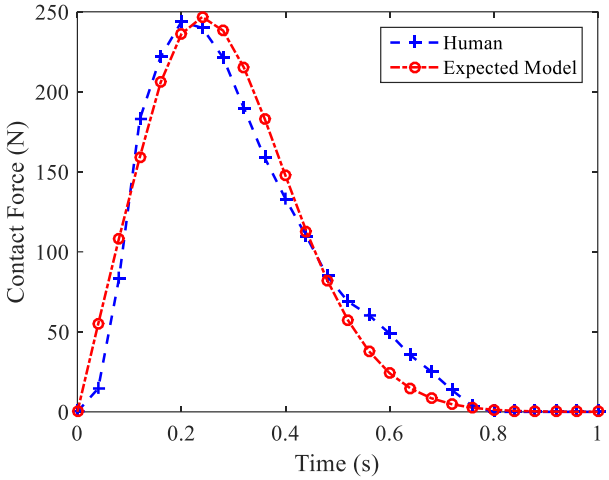

Fig. 9. Comparison of the contact forces of the humanoid model that uses the spring-damper system and a human.

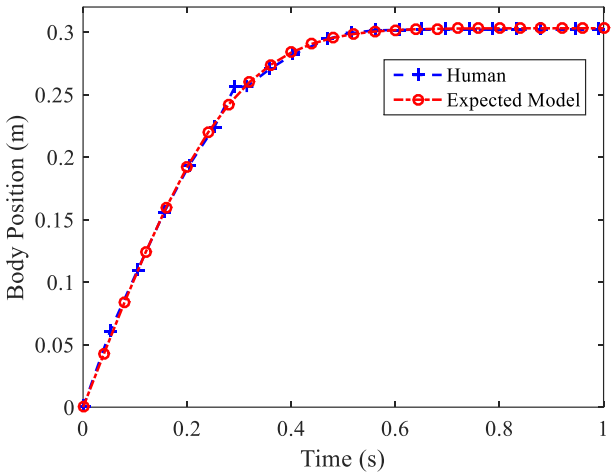

Fig. 10. Comparison of the body positions of the humanoid model that uses the spring-damper system and a human.

The dynamics of the humanoid model that uses the spring-damper system are similar to those of the human arm. According to the equivalence law of dynamic responses, the spring-damper system has achieved accurate dynamic modeling of the human arm, so it can be used as the expected control model for robot astronaut humanoid parking.

III. Robot Astronaut Parking Control Based On Human Body Dynamics

The expected control model developed in Section II is considered to be the intermediate connector in the robot astronaut control system; it maps the human parking dynamics to the robot parking control, which allows the robot to perform stable humanoid parking. This section introduces the control of stable parking of a robot astronaut based on human dynamic characteristics.

A. Dynamics Model of a Robot Astronaut

From its physiological and histological aspects, the astronaut parking process is an interactive process involving the arm muscles, ligaments and bones. In this process, the torso, upper arm, forearm and hand make up a planar moving structure with six linkages, including two sets of three linkages symmetrically connected to the torso [27]. Referring to this, the robot parking model was simplified as shown in Fig. 11.

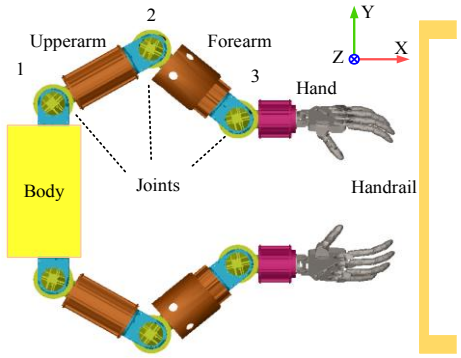

Fig. 11. Collision between the simplified model of a dual-arm robot and a space station cabin handrail. In this model, the body is equivalent to the torso of the robot astronaut, joint 1 is equivalent to the shoulder joint of the robot astronaut, joint 2 is equivalent to the elbow joint, and joint 3 is equivalent to the wrist joint. The total robot mass is equal to the mass of the astronaut.

The symbols used in this model are defined in TABLE I.

TABLE I
Main Symbols Used in This Paper

Definition	Symbol
Robot rod number	$i = 0,\ 1,\ 2,\ 3$
Robot's left (right) arm coordinate system	Σ_l (Σ_r)
Robot's body coordinate system	Σ_0
Coordinate system of the center of mass (COM) of the robot rod	Σ_{ci}
Robot's joint coordinate system	Σ_i
Normal direction of the coordinate system	Σ_x
Tangent direction of the coordinate system	Σ_y
Joint i angular variable	θ_i
Driving torque of the joint motor	$\boldsymbol{\tau}_{out}$

In the table, the subscript i represents the rod number; $i = 0$ represents the robot body itself, and 1, 2, and 3 indicate the joint numbers of the left (right) arm of the robot.

B. Mapping between Human Dynamics and Robot Astronaut Dynamics

1) Dynamics Mapping Analysis

The astronaut parking process can be interpreted as a process in which the human body's momentum gradually decreases to zero due to the pressure of a contact force. During this process, the momentum of the system composed of the human and the space station is conserved. In terms of the robot astronaut, if the contact force on the end of the arm during parking is equal to the contact force of the expected model, according to momentum conservation, we have the following:

$$\int f_{contact} dt = \int m dv \tag{11}$$

where m represents the total mass of the robot astronaut, the velocity of the robot varies in real time according to the velocity of the expected model. Therefore, after the real-time mapping of the contact force between the human body and the robot astronaut, the robot astronaut could theoretically perform parking in accordance with the variation in velocity of the astronaut during parking, and the dynamic mapping of parking from the human body to the robot astronaut could be realized.

However, in actual parking, it is difficult for single contact-force mapping to ensure that the robot astronaut can perform stable parking based on the expected dynamic characteristics. There are three main causes for this, as follows:

a) Difference in the Mass Distribution

In the expected model, the system mass is concentrated in the mass block, and its spatial position relative to the system's COM does not change. The mass of the robot is distributed in the torso, upper arm, and forearm, and the spatial mass distribution varies in real time with the bending of the arm. Because of the mass distribution, the robot may exhibit dynamic characteristics of "over-stiffness" or "over-flexibility", which can result in a rigid collision of the robot

with the handrail or make it unable to decelerate in time, which would lead to a collision between the body and the handrail.

b) The Influence of the Tangential Velocity

Affected by the workspace, robot motion, and environmental disturbances, the robot often has an initial velocity in both the X and Y directions simultaneously. A single X-direction contact force mapping can only achieve the parking control of the robot in the X direction. Meanwhile, the initial velocity in the Y direction causes a tangential displacement of the center of mass of the robot. At this time, the robot could rotate around the center of mass under the torque of the contact force. As the tangential displacement of the center of mass increases, the angle of rotation could continue to increase; eventually one arm of the robot could separate from the bulkhead, and the other arm could have an unintended rigid collision with the bulkhead.

c) Cumulative Effect of Small Errors in Force Mapping

The robot astronaut is affected by the internal forces of the mechanical structure, external disturbance forces, and multipoint collision forces on the end of the arm during parking. Its dynamic behavior is complicated, which results in slight deviations $\delta_{t,\,dynamics}$ between the real-time dynamic characteristics expressed by the robot and the expected dynamic characteristics. The cumulatives of $\delta_{t,dynamics}$ over time leads to increasing differences between the actual and expected dynamic characteristics of the robot.

Therefore, the complete parking control system is divided into the following three parts: normal contact force mapping, tangential parking control, and real-time velocity mapping. The normal contact force mapping realizes the mapping from the human contact force to the robot normal contact force; tangential parking control realizes the control of the tangential motion, force and robot orientation; real-time velocity mapping compensates the small differences in model quality and contact force mapping and achieves a complete mapping from the human body to the dynamic characteristics of the robot astronaut.

2) Normal contact force mapping

During the human parking, the dynamic characteristics of human motion and force are concentrated in the X direction, so the X direction is regarded as the main direction of the robot astronaut parking. In this direction, it is assumed that the robot is not subject to any external force other than the contact force of the handrail. If the end contact force of the robot is equal in value to the end contact force when the human body is parked, then equation (11) can be rewritten as follows:

$$\int f_{x,\,contact}dt = \int mdv_x \,. \tag{12}$$

In other words, the X-direction velocity of the robot will change with the same trend of the X-direction velocity of the human body, and finally achieves a humanoid parking.

At time *t* during parking, the robot's Jacobian matrix can be obtained according to the joint angle via sensor feedback. At this time, the desired driving torque of the joints are as follows:

$$\boldsymbol{\tau} = \mathbf{J}^T\mathbf{F} \tag{13}$$

where $\boldsymbol{\tau}$ represents joint calculation torque, $\mathbf{F} = [f_{x,\,contact} \quad f_{y,\,contact} \quad 0]^T$ indicates the end contact force of the robot. According to the above mapping rules, the normal contact force mapping from the desired model to the robot is realized. According to equation (12), the final momentum of the robot will decay to zero.

3) Tangential parking control

In actual parking, the robot often has a tangential initial velocity. It is difficult for one-dimensional normal contact-force mapping to ensure that the robot astronaut can perform stable parking. On this basis, tangential parking control is introduced to the control system. The tangential parking control of the robot mainly realizes the following two major functions: tangential velocity control and robot attitude control.

When the tangential initial velocity of the robot is v_{y0}, the end of the robot touches the handrail and generates relative displacement. At this time, the end tangential contact force is the sliding friction force [28] as follows:

$$f_{y,\,contact} = \mu_k f_{x,\,contact} \tag{14}$$

where μ_k is the coefficient of dynamic friction.

Under the sliding friction force, the tangential velocity of the end of the robot is quickly attenuated to zero. And the end contact force of the robot becomes static friction, as follows:

$$f_{y,\,contact} < \mu_s f_{x,\,contact} \tag{15}$$

where μ_s is the coefficient of static friction.

Define a scaling factor $k_f < \mu_k < \mu_s$, and let $f_{y,\,contact} = k_f f_{x,\,contact}$. Multiply both sides of equation (12) by k_f to obtain the followings:

$$\int k_f f_{x,\,contact}dt = \int k_f mdv_x = \int f_{y,\,contact}dt = \int mdv_y \tag{16}$$

Because the main mass of the robot is concentrated in the torso, its tangential velocity attenuation mainly depends on the static friction impulse. Therefore, the torso velocity is satisfied $v_y = k_f v_x$ at time t during parking, and the stable control of the tangential velocity is achieved accordingly.

When the tangential velocity of the end of the robot is zero, the robot's torso still has a large tangential velocity. At this time, the center of mass of the robot is no longer on the centerline of the two arms. Under the normal contact force of the two arms, the robot could rotate around the center of mass.

At time t during parking, the robot's torso rotation angle is θ_0, and the angular velocity is ω_0. According to this, PD feedback control is performed on the normal contact force of the two arms.

$$\Delta f_x = k_p\theta_0 + k_d\omega_0 \,. \tag{17}$$

Redistributing the normal contact force of the arms as follows:

$$f_{x,\,l,\,contact} = \frac{1}{2} f_{x,\,contact} + \Delta f_x \tag{18}$$

$$f_{x,\,r,\,contact} = \frac{1}{2} f_{x,\,contact} - \Delta f_x \,. \tag{20}$$

The attitude control of the robot during the parking is realized under the premise of not affecting the motion control of the main direction of the robot.

4) Velocity Mapping

Velocity mapping is the dynamic compensation for the force mapping. The dynamic characteristics of the robot are directly affected by the contact force on the end of the arm and the driving torques of the joints, the contact force on the end of the arm is determined by the motion characteristics of the robot, and the motion characteristics of the robot are ultimately affected by the driving torques of the joints. Therefore, the compensation effect of the velocity mapping should be reflected in the driving torques of the joints; that is,

$$\boldsymbol{\tau}_{out}(t) = \lambda \boldsymbol{\tau}(t) \tag{20}$$

where λ is the compensation factor, which is generated by the velocity mapping.

Because the force, velocity, and body position of the robot astronaut change dynamically during parking, the compensation factor λ of the robot astronaut during parking should be determined uniquely according to the system's dynamic characteristics at the current moment; that is, the compensation factor should have a self-adaption ability that corresponds to the characteristics of the system to ensure that the velocity mapping can achieve an ideal compensation effect at any time during the parking process. This paper introduces PD control through the dynamic error between the actual velocity of the robot and the expected velocity, which can actively adjust λ to achieve self-adapted regulation of the compensation factor based on the dynamic characteristics of the system.

The difference between the velocity of the expected model $v_d(t)$ and the actual velocity from the robot astronaut dynamic model $v(t)$ is as follows:

$$\Delta v(t) = v_d(t) - v(t) . \tag{21}$$

According to the incremental PD algorithm,

$$\Delta\lambda(t) = k_p(\Delta v(t) - \Delta v(t-\Delta t_c)) + k_d(\Delta v(t) - 2\Delta v(t-\Delta t_c) + \Delta v(t-2\Delta t_c)) \tag{22}$$

where Δt_c is the control step size.

The compensation factor is updated at that moment as follows:

$$\lambda(t) = \lambda(t-\Delta t_c) + \Delta\lambda(t) . \tag{23}$$

The above three control subsystems realize the contact force mapping and velocity mapping from the expected model to the robot system, and thus the robot astronaut humanoid parking control system based on the human parking dynamics is obtained as shown in Fig. 12.

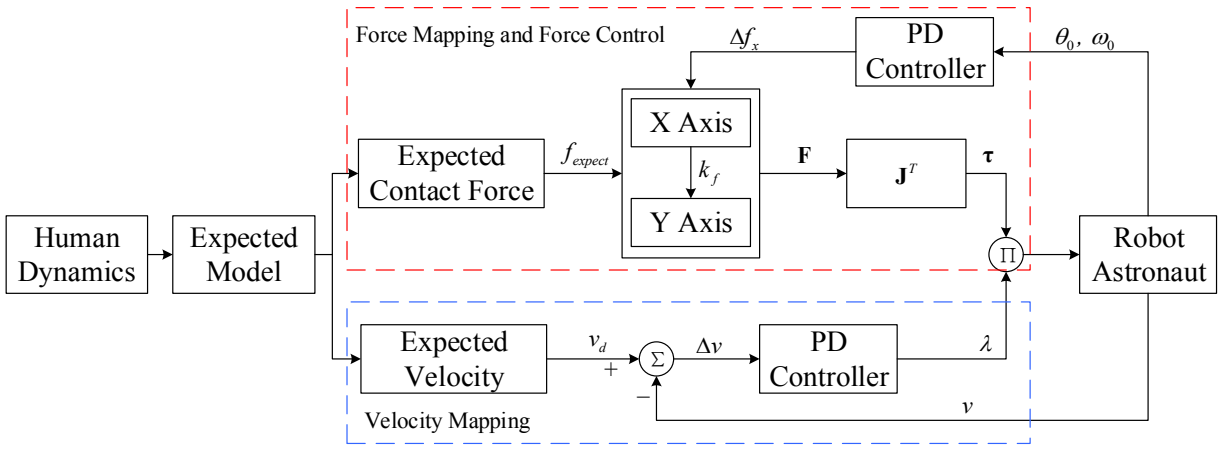

Fig. 12. Mathematical mapping from the expected model to the control system of the robot astronaut. The upper part of the figure shows the force mapping based on human dynamics and the force control for the Y-axis, and the lower part shows the velocity mapping based on the PD feedback control. Through the two mappings, the mapping of human dynamics to the control of robot astronaut parking is performed using the expected model.

The ideal response model of the control system in this paper is the expected model established using the spring-damper system. The stability of the expected model directly determines the stability of the control system. For the variable parameter spring damping system used in the modeling part, all the physical parameters are positive definite, so the control system in this paper is stable.

IV. Evaluation Method Of Humanoid Robot Astronaut Parking

The dynamic characteristics of human parking under microgravity are important criteria for evaluating humanoid robot astronaut parking. After comprehensively considering the key characteristics of the human and the robot during parking, such as the contact force, stabilization time, body position and velocity fluctuation, this paper presents a method for evaluating humanoid robot astronaut parking.

Astronauts can protect themselves from injury when they are parking in a space station because they can ensure that the contact force is always within a reasonable range through the flexibility of their arm. The original intention of adopting humanoid control for robot parking is for the robot to exhibit the same "flexibility" as human beings and ensure the stability of the robot's mechanical mechanism and safe interactions with the space station during parking. Therefore, the contact force is the primary evaluation index.

The analysis of the effect of the force shows that a significant force effect is produced only when the force exceeds the safety

limit, and there is a certain action time. Therefore, during parking, damage to the robot or the space station occurs when the contact force is too large and lasts for a certain period of time, so that the impulse of the contact force is much larger than the momentum of the robot, and a rigid collision occurs between the robot and the handrail. We select the peak force in human parking to be f_h and introduce the contact force evaluation function as follows:

$$\Gamma_f = \alpha \frac{\left| f_{r,\max} - f_{h,\max} \right| + f_{h,\max}}{f_{h,\max}} \tag{24}$$

where α is the weight of the contact force in the evaluation; $f_{r,\max}$ is the maximum contact force on the end of the robot arm during parking; and $f_{h,\max}$ is the maximum contact force on the end of the human arm during parking.

Time is a direct evaluation of the efficiency of the robot astronaut parking. According to the momentum theorem, it is always possible to obtain a smaller average contact force by extending the contact time during parking. However, a long stabilization time does not meet the efficiency requirement of the wide range of motion of the robot astronaut. This paper proposes a time evaluation function for the parking of the robot astronaut from the perspective of motion efficiency as follows:

$$\Gamma_t = \beta \frac{t_{r,d}}{\left| t_{r,d} - t_{h,d} \right| e^{1.5(t_{r,d} - t_{h,d})} + t_{r,d}} \tag{25}$$

where β is the weight of time in the evaluation method, $t_{h,d}$ is the stabilization time of human parking (the parking is viewed as being in a stable state when the contact force is less than 0.01 N), and $t_{r,d}$ is the actual stabilization time of the robot parking. When $t_{r,d} = t_{h,d}$ and $\Gamma_t = \beta$, the robot astronaut can be considered an ideal humanoid robot in terms of the stabilization time; when $t_{r,d} > t_{h,d}$, Γ_t increases exponentially, which indicates that the efficiency of parking decreases.

In robot astronaut parking, the maximum displacement of the body is limited by the mechanical structure and arm posture. If the theoretical displacement of the robot body during parking is large, the steady state of the robot might be in the position shown in Fig. 13. The mechanical structure of the various parts of the robot arm may cause interference. When $d \to 0$, the robot arm will reach a singular pose, which causes the robot body to collide directly with the handrail, resulting in a failure to park.

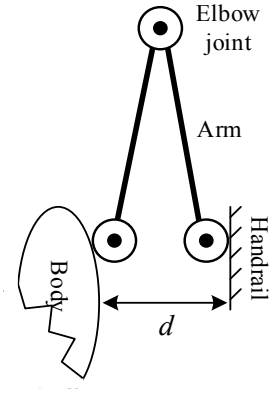

Fig. 13. The final steady-state of one arm of the robot when the displacement is too large.

A piecewise function based on the actual configuration of the robot is introduced to evaluate the displacement characteristics of the robot, as follows:

$$\Gamma_s = \begin{cases} \gamma \dfrac{s_r}{s_h} & s_r < s_{\max} \\ +\infty & s_r \geq s_{\max} \end{cases} \tag{26}$$

where γ is the weight of the displacement in the evaluation, s_r is the robot stable state parking displacement, s_h is the human stable state parking displacement, and $s_{\max}$ is the maximum theoretical displacement determined by the configurations of the robot (in this paper, $s_{\max} = 0.433$ m). When the robot parking displacement exceeds $s_{\max}$, the robot may be in a strange position, or mechanical structural interference may occur, and the parking is deemed to have failed.

One of the main research focuses of this paper is to make the robot perform more like a human during parking. The velocity of a human during parking is even and continuous, and there are no sudden changes in acceleration. The intensity of the change in velocity is also an important indicator to evaluate the humanoid robot parking. An evaluation function for the velocity of the robot parking is introduced as follows:

$$\Gamma_v = \eta \left\{ \frac{(\sum_i^N v_{ri} - \bar{v}_{ri})^2}{(\sum_i^N v_{hi} - \bar{v}_{hi})^2} + \left| \frac{(\frac{dv_r}{dt})_{\max} - (\frac{dv_r}{dt})_{\min}}{(\frac{dv_h}{dt})_{\max} - (\frac{dv_h}{dt})_{\min}} \right| \right\} \tag{27}$$

where η is the weight of the velocity in the evaluation system; v_h is the body velocity of the human during parking; v_r is the robot astronaut's body velocity; and $N = 300$ indicates that 300 samples are taken at equal intervals from the robot astronaut parking data.

Comprehensively considering the weighting coefficients of the different evaluation indicators in the humanoid robot stable parking, the weight coefficients of the contact force, time, body position and velocity are set to α=40%, β=20%, γ=25%, $\eta = 15\%$ respectively. The total parking evaluation function is as follows:

$$\Gamma = \Gamma_f + \Gamma_t + \Gamma_v + \Gamma_s \tag{28}$$

When the robot exhibits dynamic characteristics that are

completely consistent with those of a human during parking, Γ takes the optimal value of 1. In general, the closer Γ is to 1, the better the humanoid robot parking is; the larger the difference between Γ and 1, the worse the humanoid robot parking is. When $\Gamma \to 1$ or $\Gamma \to 1$, the robot parking has failed.

V. Simulation Experiment Verification

Four types of parking simulations under microgravity are carried out in this section, i.e., humanoid parking, parking with different velocities, parking with different masses and parking with XY initial velocity. The simulations are used to verify the effectiveness, robustness and adaptiveness of the parking control method.

A. Design of the Simulation Verification System

A virtual prototype model of the robot astronaut parking simulation is designed as shown in Fig. 11. The mass of the tester providing the parking data is 80.0 kg; based on the adult body weight ratio [29], the torso mass of the robot astronaut is set to 67.0 kg, the forearm mass is 3.25 kg, the combined mass of the arm and hand is 3.25 kg, and the following assumptions regarding the robot astronaut are made:

a) the robot is bilaterally symmetrical, and the mass of each part is evenly distributed;
b) the robot in the parking remains in the same plane;
c) the wrist joint is a slave joint and does not participate in torque control;
d) the shape of the hand has little effect on the parking.

The experiment is based on the simulation platform composed of ADAMS and MATLAB. In MATLAB, the expected contact force and the expected velocity of the torso are obtained by the expected model. The driving torque on the joint is calculated by normal force mapping, tangential parking control and velocity mapping and is input into ADAMS to drive the robot virtual prototype. The simulation verification system is shown in Fig. 14.

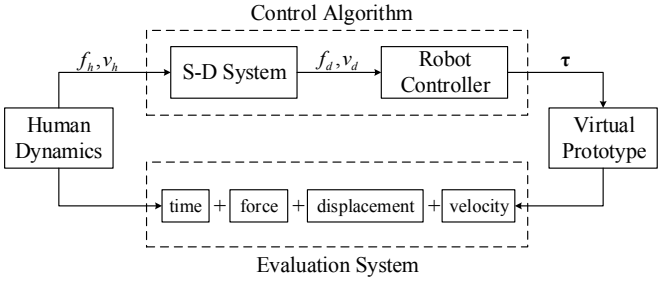

Fig. 14. Experimental verification system for humanoid robot astronaut parking. Human Dynamics represents the dynamics of the human acquired through the experiment, and the S-D System represents the expected model established by the spring-damper system.

In the virtual prototype, the contact model between the end of the robot arm and the handrail is preset in ADAMS as follows:

$$f_{contact} = \begin{cases} 0 & q > q_0 \\ k_a (q_0 - q)^{e_a} - c_a (\frac{dq}{dt}) \cdot \frac{q - q_0}{d} & q \le q_0 \end{cases} \quad (30)$$

where q_0 is the initial distance between the end of the robot arm and the handrail; q is the actual distance; k_a is the stiffness coefficient; e_a is the collision index; c_a is the maximum damping coefficient; and d is the maximum mutual penetration depth. The contact parameters are determined according to the material properties of the robot astronaut and the handrail and are shown in TABLE II.

TABLE II
Parameters of the Contact Model between Robot and Handrail in Virtual Prototype.

Contact objects	k_a (N/ m)	c_a (N·s/ m)	d (m)	e_a
Robot astronaut Space station	2.855×10^{6}	2.8×10^{4}	1.0×10^{-4}	1.5

B. Simulation Verification of Robot Astronaut Parking

To verify the effectiveness of the parking control algorithm, the following three types of parking simulations were designed: humanoid parking experiments, parking experiments with different velocities, and parking experiments with different masses, as shown in TABLE III. The coordinate system directions are defined with reference to Fig. 11 and the contact force and velocity in the figures are all the X direction data unless otherwise indicated.

TABLE III
Simulations Verification of the Control Theory of Humanoid Robot Astronaut Parking.

Exp	Name	Description
B.1)	Humanoid parking	Verification of the effectiveness of the parking control theory on the humanoid dynamics of the robot astronaut
B.2)	Parking with different velocities	Verification of the effectiveness of the parking control theory for different robot astronaut velocities
B.3)	Parking with different masses	Verification of the effectiveness of the parking control theory for different robot astronaut masses
B.4)	Parking with initial velocities in both the X and Y directions	Verification of the effectiveness of the parking control theory for the robot with XY initial velocity

1) Verification Simulation of Humanoid Parking

To verify the effectiveness of the control theory of humanoid robot astronaut parking, this paper conducts a parking simulation with a robot astronaut with the same velocity and mass as a human. The initial velocity of the robot astronaut is set to 1.0716 m/s based on the observed initial velocity of the tester before the parking. Based on the parking time of the tester, the simulation time is set to 1.0 s. The joint driving torque of the left arm of the robot astronaut is shown in Fig. 15.

Under this control torque, the robot astronaut parked successfully in simulation. The characteristics of the contact force of the robot astronaut with the handrail during this process are shown in Fig. 16.

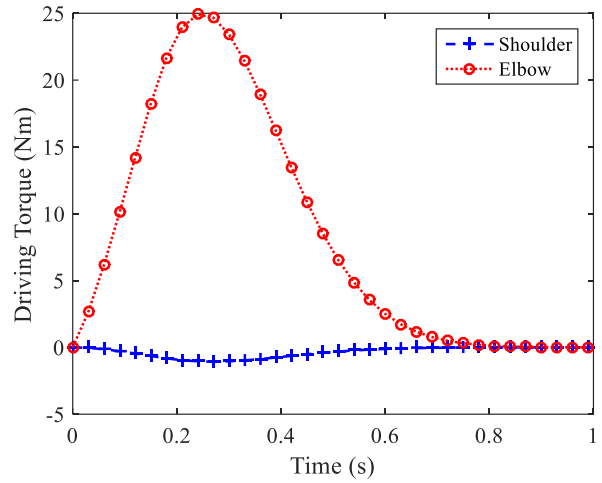

Fig. 15. Driving torques of the shoulder and elbow joints of the left arm of the robot astronaut under the humanoid parking model.

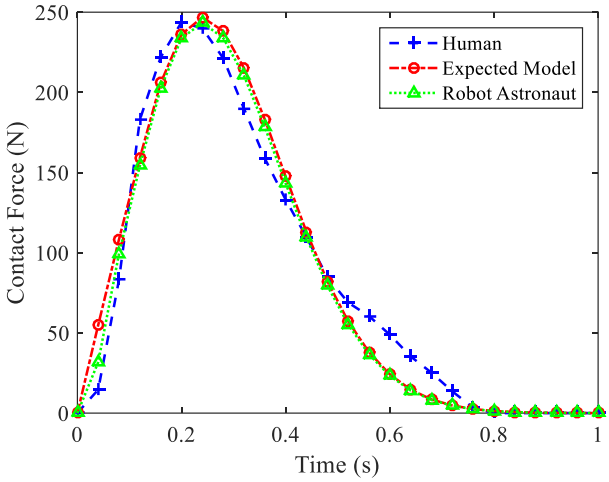

Fig. 16. Comparison of the contact forces of the human, expected model, and robot astronaut when parking with the same velocity.

The curve of the robot body's position is shown in Fig. 17.

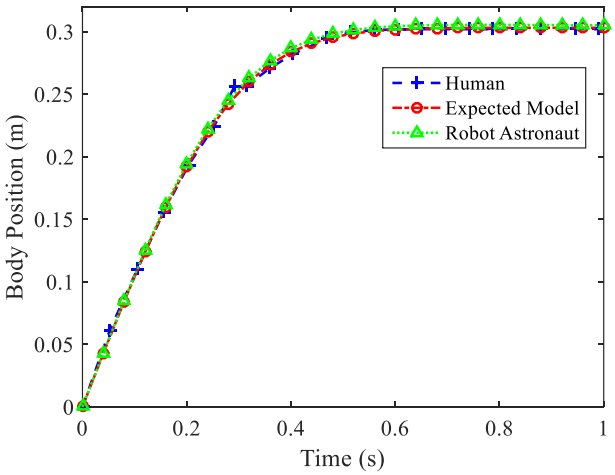

Fig. 17. Comparison of the body positions of the human, the expected model, and the robot astronaut when parking with the same velocity.

The three curves in Fig. 16 have highly similar trends, and the dynamics can be divided into two phases. In the elastic phase, the contact force gradually increases from zero to a peak. During the damping phase, the contact force decrease to zero. The system reaches a steady state, which conforms to the idea of humanoid stable parking. In Fig. 17 , the trends of the body positions of the human, the expected model and the robot astronaut are identical, which indicates that the control system achieved good stable humanoid parking.

The control of the humanoid robot astronaut parking is not only consistent in terms of the dynamics, but the consistency of the changes in the arm orientation between the human and the robot is also an important manifestation. The changes in the joint angle of the human arm and the robot arm are shown in Fig. 18.

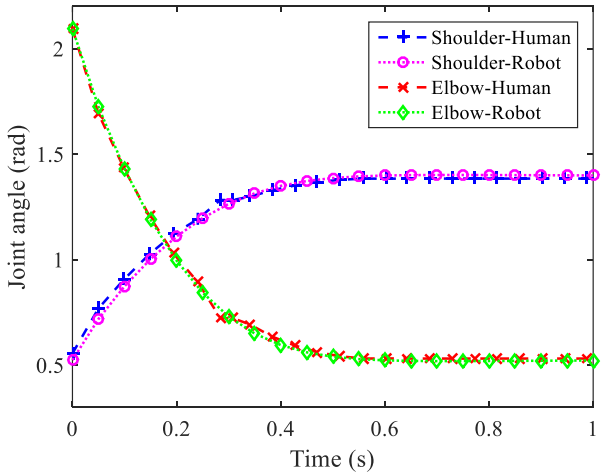

Fig. 18. Comparison of the changes in the joint angles of the human and robot astronaut during parking. Joint1 represents the shoulder joint, and Joint2 represents the elbow joint. Due to the unique configuration of the robot, the angles of the shoulder joint and the wrist joint are nearly identical during the parking. Only the shoulder and elbow angles are shown in the figure.

By further extracting the simulation data related to the evaluation function, the evaluation of each indicator of the parking is obtained, as shown in TABLE IV.

TABLE IV
ANALYSIS OF THE KEY DATA OF THE ROBOT ASTRONAUT UNDER THE CONTROL OF THE HUMANOID MODEL.

Evaluation method	Human	Expected model	Robot
Contact force (N)	247.0	246.8	246.5
Stabilization time (s)	0.785	0.924	0.916
Velocity fluctuation (m/s^2)	-3.238	-3.321	-3.32
Parking distance (m)	0.3373	0.3311	0.3101
Parking effect (Γ)	1.0	1.034	1.016

The results presented in the table show that the evaluations of the parking of the expected model and the robot astronaut are very close to the optimal value of 1.0, which indicates that the humanoid control theory enables the robot astronaut to achieve a highly stable humanoid parking.

2) Parking Simulation with Different Velocities

To verify that the control system can achieve stable parking of robots with different velocities, a robot parking simulation with different velocities is designed. Because the range of the robot's motion in the cabin is limited, for the sake of safety, this paper assumes that the velocity of the robot astronaut in a single direction in the cabin does not exceed 3.5 m/s. The low, medium and high velocities are 0.8, 2.0, and 3.5 m/s, respectively, which

are the initial velocities before the parking occurs. The mechanical structure, mass distribution, and joint configuration of the robot remained unchanged during the simulation. The corresponding characteristic parameters of the expected model are obtained based on the initial velocity of the robot astronaut, as shown in TABLE V, in which k is the initial spring stiffness, c is the final system damping coefficient, and t_s is the time when the mixing phase begins.

TABLE V
EXPECTED MODEL PARAMETERS OF ROBOT ASTRONAUT AT DIFFERENT INITIAL VELOCITIES.

Total Mass (kg)	v_0 (m/s)	k (N/m)	t_s (s)	c_{t_s} (N·s/m)	s_c
80.0	0.8	1440	0.14	227.12	1.50
80.0	2.0	3600	0.05	183.04	4.27
80.0	3.5	6300	0.03	186.84	13.07

The attributes of the robot astronaut, such as the mass distribution and joint configuration, do not change with changes in the initial velocity. In the velocity mapping the PD parameters are set according to the difference in the mass distribution between the expected model and the robot model, so the control system uses the same set of PD parameter, where $k_p = 20.0$, $k_d = 0.01$.

The contact forces of the parking simulation with different initial velocities are shown in Fig. 19.

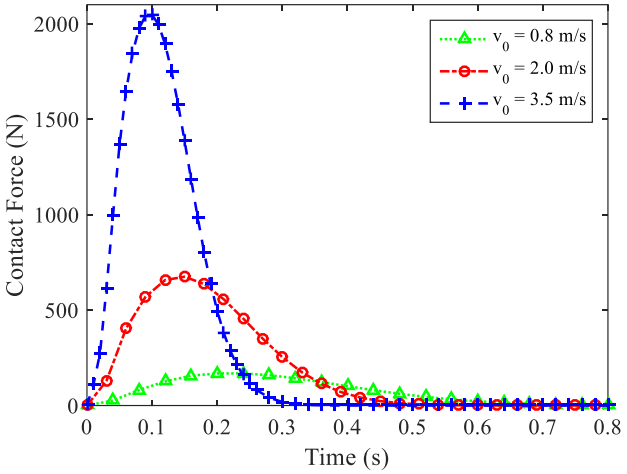

Fig. 19. Comparison of the contact forces between the expected model and the end of the robot astronaut's arm during parking with initial velocities of 0.8, 2.0, and 3.5 m/s. When the initial velocity of the robot astronaut increases, the contact force between the robot and the handrail also increases; this is because of higher the velocity is, the greater the robot's momentum is, and thus the greater the contact force is.

The body position of the robot astronaut during parking with different initial velocities are shown in Fig. 20.

In the simulation, the robot astronaut achieved stable and rapid parking at different initial velocities, which indicates that the control system has the ability to adapt to the different initial velocities of the robot and verifies the robustness of the control system when the initial velocity of the robot changes.

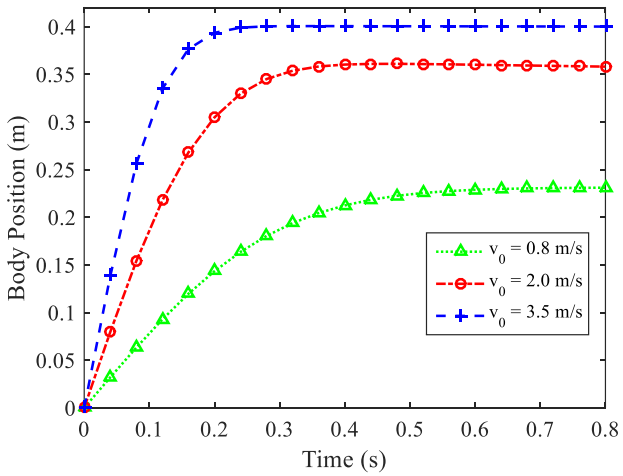

Fig. 20. Comparison of the body positions of the expected model and the robot astronaut at different initial velocities (0.8, 2.0, and 3.5 m/s).

3) Parking Simulation with Different Masses

To verify that the proposed control theory can achieve the ideal parking control for robots with different masses, robot parking simulations with different masses are designed. Masses of 60, 80, and 100 kg were used for the robot astronaut, and virtual prototype models of the robots with different total masses and moments of inertia were obtained. The control system obtains the corresponding characteristic parameters according to the different masses of the robot astronaut, as shown in TABLE VI.

TABLE VI
EXPECTED MODEL PARAMETERS OF ROBOT ASTRONAUTS WITH DIFFERENT MASSES

Total Mass (kg)	v_0 (m/s)	k (N/m)	t_s (s)	c_{t_s} (N·s/m)	s_c
60.0	2.0	2700	0.05	137.28	3.42
80.0	2.0	3600	0.05	183.04	4.57
100.0	2.0	4500	0.05	228.80	5.71

The contact forces of the robot astronauts with different masses during parking are shown in Fig. 21.

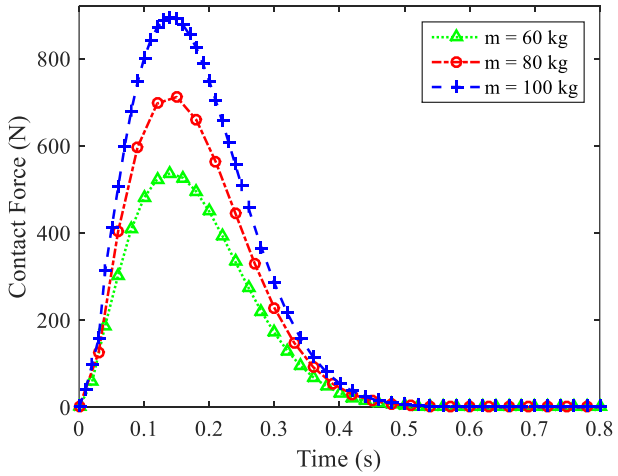

Fig. 21. Contact forces of the end of the robot arm during parking with different astronaut masses (60, 80, and 100 kg). At the same initial velocity, as the mass of the robot astronaut increases, the momentum also increases; therefore, under the same contact conditions, the impulse of the contact force also increases,

which is reflected in the curve as the overall increase in magnitude of the contact force.

The body positions and body velocities are shown in Fig. 22. Although the masses and moments of inertia of the robot astronaut in the figure are different, the velocities of the astronauts in the simulation gradually attenuate to zero with the same trend and achieve stable and rapid parking. This shows that the control system has the ability to adapt to different robot masses, which verifies the robustness of the control system when the robot mass is disturbed.

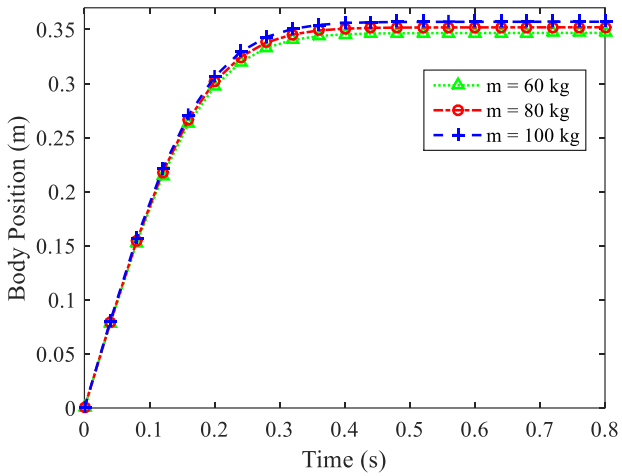

Fig. 22. Body positions of robot astronauts with different masses (60, 80, and 100 kg) during parking.

4) Simulation of Parking with Initial Velocities in the X and Y Directions

This simulation is used to verify that the control system can achieve stable humanoid parking for robots with initial velocities in both the X and Y directions. Limited by the length of the robot arm and the friction coefficient between the arm and the handrail contact surface, the velocity in the Y direction that can be controlled by the control system is approximately 30% of the velocity in the X direction. The experimental specific parameters are set as follows:

The design mass of the robot virtual prototype is 67.0 kg, the initial velocity in the X direction is 1.0716 m/s, and the initial velocity in the Y direction is 0.3 m/s. The material properties of the contact between rubber and steel are used for the contact between the end of the robot and the handrail, including the static friction coefficient $\mu_s = 0.8$ and the dynamic friction coefficient $\mu_k = 0.76$. The control expected model used in the X direction is shown as TABLE VII.

TABLE VII
EXPECTED MODEL PARAMETERS OF ROBOT ASTRONAUT WITH X AND Y INITIAL VELOCITIES

Total Mass (kg)	v_0 (m/s)	k (N/m)	t_s (s)	c_{t_s} (N·s/m)	s_c
67.0	1.0716	1615	0.13	241.60	1.5

The robot astronaut successfully realized stable humanoid parking with initial velocities in the X and Y directions. The driving torques on the left and right arm joints are shown in Fig. 23.

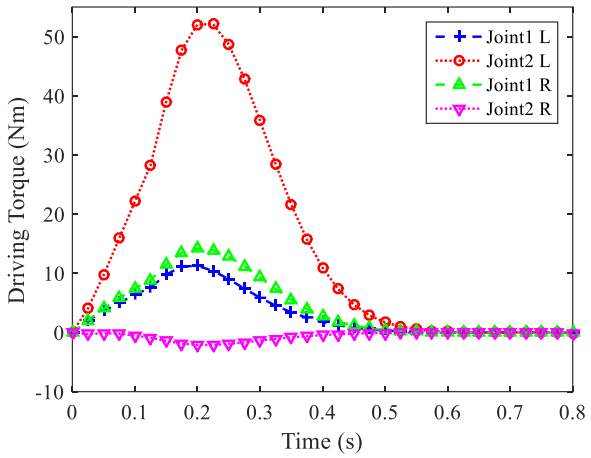

Fig. 23. The driving torque of left and right arms joints 1 and 2. Joint1 is the shoulder joint, Joint2 is the elbow joint, L represents the left arm, and R represents the right arm. Due to the Y-direction velocity and friction, the torques on the arms are no longer equal.

The left and right arm contact forces in the main parking direction –X direction are shown in Fig. 24.

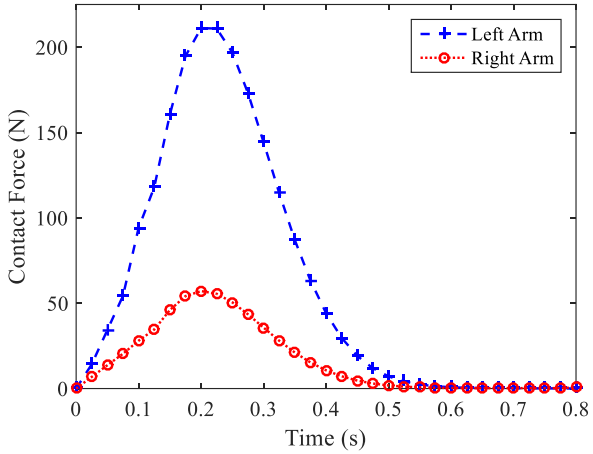

Fig. 24. The contact forces of the left and right extremities of the robot. Because of the velocity in the Y direction, the robot has a movement toward the center of mass and the left arm, so the left arm contact force is significantly larger than the right arm contact force.

Variation of the torso velocity in the X and Y directions during the parking simulation are shown in Fig. 25.

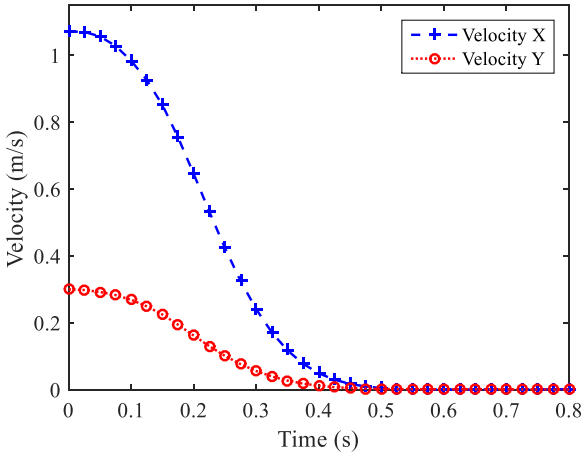

Fig. 25. The variation curve of robot velocities in the X, Y directions. Under the action of the control system, the attention of the X and Y velocities of the robot follows the velocity change curve of the human astronaut during parking, which reflects the continuity and stability of the stable parking.

The orientation angle of the robot torso is shown in Fig. 26.

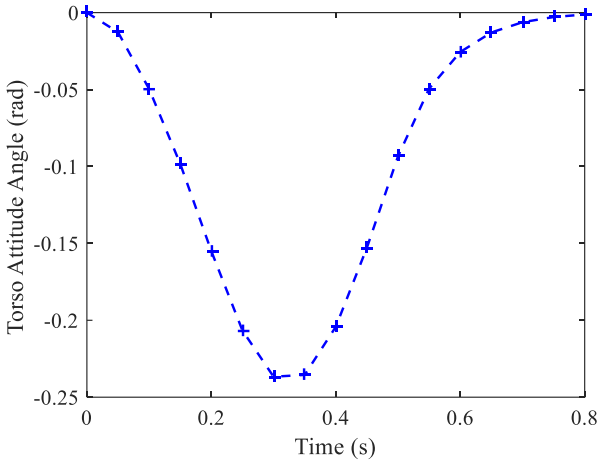

Fig. 26. Variation of the torso's orientation angle. At the initial moment, the velocity in the Y direction is relatively large, and at this time the distribution of the contact force of the arms in the X direction is relatively small, and the suppression effect on the rotation of the robot is weak. As time increases, the anti-rotation torque generated by the contact force of the arms gradually increases, and finally the robot's orientation is controlled to the expected positive direction.

5) Discussion of Three-Dimensional Parking

Human parking is mainly the movement process of the human under the action of the X-direction contact force and the YZ direction friction force. Therefore, this study mainly considers the contact force and friction between a human and the handrail, and does not consider the torsional moment generated by the human hand while grasping the handrail. For the three-dimensional parking, the Z-direction control is in the same as the Y-direction control method. However, the absence of torsional moment can only achieve the Z-direction velocity control, and the attitude control cannot be realized. The real robot system can provide a torsional moment by grasping the handrail, thus enabling a stable stop of the robot with an initial velocity in the Z direction. In the future, we will develop an experimental robot platform where the robot can grasp the handrail of the space station, which will be used to verify the parking results.

In summary, the parking control system in this paper not only enables the robot astronaut to exhibit highly humanoid dynamic characteristics during parking, and simulation achieves the stable and fast parking of robot astronauts with different initial velocities and different masses, which validates the stability and robustness of the control system. The parking control system also realizes a stable humanoid parking for the robot astronaut with initial velocities in both the X and Y directions, reflecting the adaptability of the control system.

VI. Conclusion

This paper proposed a novel wide-ranging spatial motion mode for a robot astronaut. By not changing the basic structure of the space station and using the wide-ranging motion of a human astronaut in the space station as a reference, this method realizes the wide-ranging motion of a robot astronaut through humanoid control. Focusing on the parking mode, which is a relatively complicated mode of motion, a robot astronaut parking control method based on human body parking dynamics is proposed. First, a mass-spring-damper system is used to model the dynamics of the human arms, and an expected model that is equivalent to the human dynamic response is obtained. Using the expected model as a bridge, the dynamic characteristics of the human arms during parking are then applied to the robot astronaut through normal contact force mapping, tangential parking control, and real-time velocity mapping. The control of highly humanoid and stable parking in the XY plane of the robot astronaut is realized. The simulation verifies the effectiveness, robustness and adaptiveness of the proposed humanoid parking control method.

References

[1] E. Blaber, H. Marçal, B. P. Burns, "Bioastronautics: the influence of microgravity on astronaut health," *Astrobiology*, vol. 10, no. 5, pp. 463–73, Jun. 2010.

[2] W. Bluethmann, R. Ambrose, M. Diftler, S. Askew, E. Huber, M. Goza, F. Rehnmark, C. Lovchik, and D. Magruder, "Robonaut: a robot designed to work with humans in space," *Auton. Robot.*, vol. 14, no. 2–3, pp. 179–197, Mar–May. 2003.

[3] M. P. Nagaraja, D. Risin, "The current state of bone loss research: data from spaceflight and microgravity simulators," *J. Cell. Biochem.,* vol. 114, no. 5, pp. 1001–1008, May. 2013.

[4] J. Liu, Q. Gao, Z. Liu, and Y. Li, "Attitude control for astronaut assisted robot in the space station," *Int. J. Control. Autom. Syst.*, vol. 14, no. 4, pp. 1082–1094, Aug. 2016.

[5] Diftler, A. Myron, "Robonaut 2 - Activities of the First Humanoid Robot on the International Space Station," *Mol. Phys.*, vol. 8, no. 1, pp. 39–44, Sep. 2012.

[6] Nokleby, B. Scott, "Singularity analysis of the Canadarm2," *Mech. Mach. Theory.*, vol. 42, no. 4, pp. 442–454, Apr. 2007.

[7] M. Bualat, J. Barlow, T. Fong and C. Provencher, "Astrobee: Developing a Free-flying Robot for the International Space Station," *Aiaa Space Conf. Exposition*, Pasadena, CA, USA, 2015, DOI: 10.2514/6.2015-4643.

[8] R. O. Ambrose, H. Aldridge, R. S. Askew, R. R. Burridge, W. Bluethmann, M. Diftler, C. Lovchik, D. Magruder, and F. Rehnmark, "Robonaut: nasa's space humanoid," *IEEE Intell. Syst. App.*, vol. 15, no. 4, pp. 57–63, Aug. 2000.

[9] Diftler *et al*., "Robonaut 2 - The first humanoid robot in space," in *Proc. IEEE Int. Conf. Robot. Autom.*, Shanghai, China, 2011, pp. 2178–2183.

[10] K. Ashworth, "CANADARM to the MSS - Unique verification features of the Canadian Mobile Servicing System," in *Aerospace Testing Seminar*, Manhattan Beach, CA, USA, 1991, pp. 255–268b.

[11] G. Gibbs, S. Sachdev, "Canada and the International Space Station program: Overview and status," *Acta. Astronaut.,* vol. 51, no. 1–9, pp. 591–600, Jul–Nov. 2002.

[12] P. Lanza, A. Cumani, S. Denasi, A. Guiducci, and G. Quaglia, "EUROBOT WET Model Architecture and Description of Vision Processing for Automatic Robot Control," in *Dasia 2006 – Data Syst. Aerosp.*, Berlin, Germany, 2006, ESA SP–630.

[13] Z. Y. Sun, H. Li, Z. H. Jiang, Z. Z. Song, Y. Mo, and M. Ceccarelli, "Prototype Design and Performance Tests of Beijing Astronaut Robot," *Appl. Sci-Basel.*, vol. 8, no. 8, 1342, Aug. 2018, DOI: 10.3390/app8081342.

[14] B. Wei, Z. H. Jiang, H. Li, Q. Dong, W. C. Ni, and Q. Huang, "Adaptive Impedance Controller for a Robot Astronaut to Climb Stably in a Space Station," *Int. J. Adv. Robot. Syst.*, vol.13, no. 3, 81, May. 2016, DOI: 10.5772/63544.

[15] Chung, K. Wing, "Truss Climbing Robot for Space Station: Design, Analysis, and Motion Control," Ph.D. dissertation, CUHK., HongKong, China, Jan. 2012.

[16] M. Shahbazi, R. Babuška, and G. A. D. Lopes, "Unified Modeling and Control of Walking and Running on the Spring-Loaded Inverted Pendulum," *IEEE Trans. Robot.*, vol. 32, no. 5, pp. 1178–1195, Aug. 2016.

[17] N. Motoi, T. Suzuki, and K. Ohnishi, "A Bipedal Locomotion Planning Based on Virtual Linear Inverted Pendulum Mode," in *IEEE Int. Conf. Ind. Technol.*, Bombay, India, 2007, pp. 54–61.

[18] Y. Hwang, E. Inohira, A. Konno, and M. Uchiyama, "An order n dynamic simulator for a humanoid robot with a virtual spring-damper contact model," in *IEEE Int. Conf. Robot. Autom.*, TaiPei, TaiWan, 2003, pp. 31–36.
[19] D. N. Nenchev, K. Yoshida, "Impact analysis and post-impact motion control issues of a free-floating space robot subject to a force impulse," *IEEE Trans. Robot. Autom.*, vol. 15, no. 3, pp. 548–557, Jun. 1999.
[20] S. J. Zhu, Y. F. Zheng, and Y. M. Fu, "Analysis of non-linear dynamics of a two-degree-of-freedom vibration system with non-linear damping and non-linear spring," *J. Sound. Vib.*, vol. 271, no. 1, pp. 15-24, Mar. 2004.
[21] P. Tan, W. Yan, and F. Zhou, "Experimental and theoretical study on predictive optimal control of active variable stiffness-damping system," *J. Earthq. Eng. Eng. Vib.* vol. 8, no. 1, pp. 1–4, Apr. 2007.
[22] C. C. Tsai, M. B. Cheng, and S. C. Lin, "Dynamic Modeling and Tracking Control of a Nonholonomic Wheeled Mobile Manipulator with Dual
[23] E. Suhir, "Dynamic response of a one-degree-of-freedom linear system to a shock load during drop tests: effect of viscous damping," *IEEE Trans. Compon., Packag., Manuf., Technol. A.*, vol. 19, no. 3, pp. 435–440, Oct. 1996.
[24] A. F. Vakakis, "Non-linear normal modes (nnms) and their applications in vibration theory: an overview," *Mech. Syst. Signal Pr.*, vol. 11, no. 1, pp. 3–22, Jan. 1997.
[25] A. F. Vakakis, "Analysis and Identification of Linear and Nonlinear Normal Modes in Vibrating Systems," Ph.D. dissertation, CalTech., Pasadena, CA, USA, Jul. 1990.
[26] G. Gilardi, I. Sharf, "Literature survey of contact dynamics modelling," *Mech. Mach. Theory.*, vol.37, no. 10, pp. 1213–1239, Oct. 2002.
[27] D. E. Foster, G. R. Pennock, "A study of the instantaneous centers of velocity for the 3-dof planar six-bar linkage," *Mech. Mach. Theory.*, vol. 46, no. 9, pp. 1276–1300, Sep. 2011.
[28] Y. Wang, M. T. Mason, "Two-Dimensional Rigid-Body Collisions With Friction," *J. Appl. Mech*, vol. 59, no. 3, pp. 635–642, Sep. 1992.
[29] *Inertial parameters of adult human body*, GB/T 17245–2004, May. 2004.

Zhihong Jiang was born in Jiangsu, China. He received the B.S. degree in material processing & manufacturing engineering from the Jilin University of Technology, Changchun, China, in 1998, the M.S. degree in material processing & manufacturing engineering from Jilin University, Changchun, China, in 2001, and the Ph.D. degree in electrical engineering and automation from Tsinghua University, Beijing, China, in 2005.

He is currently a Professor with the School of Mechatronic Engineering, Beijing Institute of Technology, Beijing. He is a winner of the key project of National Natural Science Foundation of China and the key project of intelligent robots in the national key research and development plan of China，and his research interests include space intelligent robotics, industry robot systems, artificial intelligence and robot vision, and human-machine interaction.

Jiafeng Xu was born in Shandong China. He received the B.S. degree in mechatronic engineering from the Beijing Institute of Technology, Beijing, China, in 2017, where he is currently working toward the M.S. degree with the School of Mechatronic Engineering. His research interests include robot motion control, robotic dynamics systems and humanoid robot systems.

Hui Li was born in Hebei, China. He received the B.S. degree in mechatronic engineering from the Hebei University of Technology, Tianjin, China, in 2005, the M.S. degree in mechatronic engineering from the Harbin Institute of Technology, Harbin, China, in 2007, and the Ph.D. degree in mechatronic engineering from the Beijing Institute of Technology, Beijing, China, in 2011.

He is currently a Associate Professor with the School of Mechatronic Engineering, Beijing Institute of Technology. His research interests include intelligent robotics, industry robot systems, artificial intelligence, and robot vision.

Qiang Huang (M'98–SM'14–F'16) was born in Hubei, China. He received the B.S. and M.S. degrees in electrical engineering from the Harbin Institute of Technology, Harbin, China, in 1986 and 1989, respectively, and the Ph.D. degree in mechanical engineering from Waseda University, Tokyo, Japan, in 1996.

He was a Research Fellow with the National Institute of Advanced Industrial Science and Technology, Tokyo, between 1996 and 1999. He was a Research Fellow with the University of Tokyo, Tokyo, between 1999 and 2000. He is currently a Professor with the Beijing Institute of Technology, Beijing, China. He is the Director of the Intelligent Robotics Institute, and the Director of the Key Laboratory of Biomimetic Robots and Systems, Ministry of Education of China.

Prof. Huang received the First Class Prize of Ministry of Education Award for Technology Invention. He serves as the chair at many IEEE conferences, such as the organizing committee chair of the 2006 IEEE/RSJ International Conference on Intelligent Robots and Systems, and the general chair of the 2017 IEEE International Conference on Robotics and Biomimetics and the 2018 IEEE-RAS International Conference on Humanoid Robotics.